PSFC/JA-98-16

Recent Progress in ICRF Physics

Miklos Porkolab[a] ,A. Becoulet,[b]
P.T. Bonoli,[a] C. Gormezano,[c]
R. Koch,[d] R.J. Majeski,[e] A. Messiaen,[d]
J.M. Noterdaeme,[f] C. Petty,[g] R. Pinsker,[g]
D. Start,[c] and R. Wilson,[e]

June 1998

Presented at the Second European Topical Conference on RF Heating and Current Drive of Fusion Devices, Brussels, Belgium, January 20-23, 1998. To be published in a Special Issue of *Plasma Physics & Controlled Fusion.*

(*a*) Massachussetts Institute of Technology, Plasma Science and Fusion Center, Cambridge, MA 02139 USA;
(*b*) Association EURATOM–CEA sur la Fusion, CEA Cadarache, 13108 St-Paul-lez-Durance Cédex, France;
(*c*) JET Joint Undertaking, Abingdon, Oxon, OX14 3EA, UK;
(*d*) Laboratoire de Physique des Plasmas–Laboratorium voor Plasmafysica, Association "Euratom–Belgium State", Ecole Royale Militaire - Koninklijke Militaire School, B–1000 Brussels, Belgium;
(*e*) Princeton Plasma Physics Laboratory, PO Box 451, Princeton, NJ 08543;
(*f*) Max-Planck-Institut für Plasmaphysik, Euratom Association, D–85748 Garching, Germany;
(*g*) General Atomics, PO Box 85608, San Diego, CA 92186

This work supported by the U.S. Department of Energy Contract No. DE-AC02-78ET51013.

RECENT PROGRESS IN ICRF PHYSICS

M. Porkolab,[a] A. Becoulet,[b] P.T. Bonoli,[a] C. Gormezano,[c] R. Koch,[d] R.J. Majeski,[e] A. Messiaen,[d] J.M. Noterdaeme,[f] C. Petty,[g] R. Pinsker,[g] D. Start,[c] and R. Wilson,[e]

(*a*) Massachussetts Institute of Technology, Plasma Science and Fusion Center, Cambridge, MA 02139 USA;

(*b*) Association EURATOM–CEA sur la Fusion, CEA Cadarache, 13108 St-Paul-lez-Durance Cédex, France;

(*c*) JET Joint Undertaking, Abingdon, Oxon, OX14 3EA, UK;

(*d*) Laboratoire de Physique des Plasmas–Laboratorium voor Plasmafysica, Association "Euratom–Belgium State", Ecole Royale Militaire - Koninklijke Militaire School, B–1000 Brussels, Belgium;

(*e*) Princeton Plasma Physics Laboratory, PO Box 451, Princeton, NJ 08543;

(*f*) Max-Planck-Institut für Plasmaphysik, Euratom Association, D–85748 Garching, Germany;

(*g*) General Atomics, PO Box 85608, San Diego, CA 92186

Abstract

Recent progress in the area of ICRF physics is examined and summarized. A very brief summary of simplified theoretical predictions is given. Illustrative examples of experimental results in the area of ICRF heating and fast wave current drive are given. ICRF heating is found to be highly effective in heating plasmas to high temperatures in modern tokamaks. Fast wave current drive has been demonstrated in several experiments and the results are in good agreement with theory. Mode conversion heating and current drive should be effective for profile control, but experimental results are still preliminary.

I. Introduction

In this paper we shall review recent progress in RF physics in the ICRF regime (Ion Cyclotron Range of Frequencies). We shall concentrate on the experimental developments in the past few years, and theoretical progress will be summarized only very briefly, and only to the extent that is necessary to understand the experimental results. Furthermore, we shall not summarize here the results obtained in DT plasmas in JET and TFTR, neither shall we say much about the use of ICRF power for attaining improved confinement regimes through profile control. These latter topics are discussed by other authors in this volume.

The main topics discussed in this paper are the following:

i. ICRF fundamental resonance minority heating regimes and second harmonic majority (and minority) heating;

ii. Direct electron heating by the Fast Magnetosonic Wave (or simply Fast Wave, or FW) by Landau/TTMP absorption;

iii. Absorption by mode conversion of the FW into ion Bernstein waves (or IBW);

iv. Current drive by the FW (or FWCD) or by the mode-converted IBW (MCCD);

v. Absorption of the FW at the higher cyclotron harmonics in the presence of energetic ions, mostly due to neutral beam injection; this may have implications for alpha particle absorption in burning plasmas;

vi. On and off-axis heating and current drive for profile control;

vii. Plasma control by ICRF power, in particular, pressure profile control, plasma rotation, MHD control;

viii. Improved confinement modes by ICRF (pellet enhanced performance, or PEP, radiative improved mode or RI, and internal transport barrier, or ITB formation with flow shear);

Although it would be desirable to give a complete review of all the experimental observations world-wide, it will be necesssary to limit the discussion here by giving only examples of different physics topics from particular tokamaks.

II. Summary of Theoretical Predictions

The propagation of the fast magnetosonic wave (or simply fast wave, or FW) is described by the dispersion relationship

$$n_\perp^2 = \frac{\left(n_\parallel^2 - R\right)\left(n_\parallel^2 - L\right)}{S - n_\parallel^2} \ , \tag{1}$$

where $n_\parallel = ck_\parallel/\omega$, $n_\perp = ck_\perp/\omega$, and R, L, and S are the usual Stix-parameters [1].

The regimes of propagation, evanescence and mode conversion for a typical minority heating case (H minority in a D plasma) in Alcator C-Mod are shown schematically in Fig. 1 (a simple slab-model is used with the toroidal magnetic field decreasing as 1/R). We see that the wave must tunnel through the evanescent region at the low field side edge, ($n_\parallel^2 = R$). The evanescent wave fields coupled to the plasma propagates beyond the $n_\parallel^2 = R$ right-hand cut-off layer as the fast wave Eq.(1),

$$\omega^2 \simeq k_\perp^2 v_A^2 \left(1 + c^2 k_\parallel^2/\omega_{pi}^2\right) \ , \tag{2}$$

where $v_A \simeq c\Omega_i/\omega_{pi}$ is the Alfvén speed. The wave arriving to the minority cyclotron resonance is absorbed by a single pass absorption factor,

$$A = 1 - e^{-2\eta} , \tag{3}$$

while a fraction $T = \exp(-2\eta)$ is transmitted.

(i.) H^+ *Minority Absorption*

For the H^+ minority resonance case we obtain [2]

$$2\eta = \frac{\pi}{2}\frac{\omega_{PD}}{c}\frac{n_H}{n_D}R . \tag{4}$$

Here n_H/n_D is the hydrogen to deuterium concentration ratio (typically a few percent).

If the minority concentration is not too high ($n_H/n_D < 0.1$) the wave is strongly attenuated as it propagates through the cyclotron resonance (and the $n_\parallel^2 = L$ cut-off layer) and is reflected from the $n_\parallel^2 = R$ cut-off layer on the high field side, resulting in multiple pass absorption. If the minority concentration is large ($> 10\%$) the $n_\parallel^2 = S$ mode conversion layer, the $n_\parallel^2 = L$ left hand cut-off layer, and the cyclotron resonance layer are well separated, and significant mode-conversion into ion Bernstein waves (IBW) may occur just on the high field side of the $n_\parallel^2 = S$ mode conversion layer. Such mode converted IBW are rapidly absorbed by electron Landau damping, offering the possibility of pressure (and possibly current) profile control [3].

(ii.) ^{3}He *Minority Absorption*

The case of ^{3}He minority in a D majority plasma is of special interest (see Fig. 2). In this case (i) significant mode conversion may occur at the $n_\parallel^2 = S$ layer since the single pass absorption on the minority ions is reduced by a factor of 1/9 as compared to the hydrogen case (due to unfavorable polarization of the wave); (ii) a second resonance ($n_\parallel^2 = S$) may occur near the plasma edge on the high field side ($\omega < \Omega_D$), offering the possibility of mode-conversion into the shear-Alfvén wave (SAW). Such unwanted resonance in relatively low-aspect ratio devices ($R/a < 3.3$) may result in edge heating, impurity generation, as well as reduced central heating.

Other absorption processes of interest include the following [2].

(iii) Majority Fundamental Resonance Absorption ($\omega = \Omega_D$)

$$2\eta = \frac{\omega_{PD}}{c}k_\parallel^2 r_{CD}^2 R , \tag{5}$$

where ω_{PD} is the deuterium angular plasma frequency, and r_{CD} is the deuterium Larmor radius. The single pass absorption efficiency predicted by Eq.(5) is usually very small (<1%).

(iv.) Cyclotron Harmonic Absorption by Majority Ions

This process is typically significant only for the second, or possibly third harmonic resonance ($\omega = \ell\Omega$). The optical depth is [2]

$$2\eta = \frac{\pi}{2}\frac{\omega_{PD}}{c}R\left(\frac{\ell^2\beta_i}{4}\right)^{\ell-1}\frac{(\ell-1)}{(\ell-2)!}\,, \tag{6}$$

which, for $\ell = 2$ reduces to

$$2\eta = \frac{\pi}{2}\frac{\omega_{PD}}{c}\beta_i R\,, \tag{7}$$

where β_i is the ion-beta.

(v.) Cyclotron Harmonic Absorption by Hot Ions

In the presence of high energy beam ions we obtain [2]

$$2\eta = \frac{\pi}{2}\frac{\omega_{PD}}{c}\left(\frac{\ell^2\beta_{h\perp}}{4}\right)^{\ell-1}\left(\frac{n_D}{n_h}\right)^{\ell-2}\frac{(\ell-1)}{(\ell-2)!}\,, \tag{8}$$

where sub-h refers to the hot (beam) component with perpendicular beta of $\beta_{h\perp}$, and density n_h. This absorption can be significant even at higher harmonics ($\ell = 6$ to 8) in the presence of high energy ions originating from neutral beams (and ultimately alpha particles).

(vi.) Direct Electron Absorption

Direct absorption of fast waves by bulk electrons can be significant in modern tokamaks with electron beta of one percent or more [2]:

$$2\eta \simeq L\frac{\pi^{1/2}}{2}\frac{\omega}{\Omega_D}\frac{\omega_{PD}}{c}\beta_e\zeta_e\exp(-\zeta_e^2) \tag{9}$$

where $\zeta_e = \omega/k_\parallel v_{te}$, $v_{te} = (2T_e/m_e)^{1/2}$, β_e is the bulk electron beta, and $L \simeq 2a/3$ is an "effective" absorption length radially where by assumption $\zeta_e \simeq 1$ (typically $\Delta L \simeq a/3$, so a total absorption length may be twice this). Typically, direct electron heating by the FW is maximum on axis, at the highest T_e region.

(vii.) Mode Conversion

Mode conversion (MC) absorption is more difficult to specify, but it may be given by a typical Budden tunneling factor 2η, such that the absorption, A is

$$A = T_B(1 - T_B) \ , \tag{10}$$

where $T_B = \exp(-2\eta)$, and the maximum value of A is 0.25 for $T_B = 0.5$. However, under certain optimal conditions a "resonator" system may be set up with significantly higher absorption efficiency [3].

(viii.) Current Drive by Fast Waves

The fast wave current drive (FWCD) efficiency has been calculated in the past by several authors [4,5]. The results may be summarized by the simple formula

$$\eta_{CD} = \frac{n_{20} I R}{P} \simeq Q T_{e10} \ , \tag{11}$$

where the density is in units of $10^{20}\mathrm{m}^{-3}$, the current in MA, the radius R in m, the power in MW, and the electron temperature in 10 keV units. The coefficient Q is in the range of 0.07–0.1 and depends on the antenna launching efficiency and off-axis electron trapping. Typically FWCD is maximized on-axis of a plasma column, where T_e is maximum.

III. Experimental Results

a. Minority Heating

The most successful minority absorption scenarios to date involve hydrogen or helium-3 minority species in the deuterium majority plasma. Among these, H^+ minority heating is very efficient, and for a typical 2-5% hydrogen concentration ratio, a single pass absorption factor of $A \gtrsim 0.8$ can be easily obtained in modern medium to large-size tokamaks. There are many examples of efficient heating with such a scenario, and here we shall simply reproduce two examples of D(H) heating. The first example is from Alcator C-Mod [6], where H-mode is efficiently obtained by this heating method (see Fig. 3). In particular, H-factors of 2.0 – 2.4 (as compared with ITER-89 scaling) are "routinely" obtained.

Another example of excellent minority heating, using the D(H) scenarios from JET [7] is shown in Fig. 4. Here 42 MHz RF frequency was used at $B = 2.6$ T, $I_p = 2.6$ MA. We see that relatively low amplitude ELMs are observed in the presence of RF heating, as opposed to the NBI injection case (see D_α signals). We see that ICRF heats as well, or better than NBI in the present case, with an H-factor of 2.0 – 2.3 (as compared to ITER-89 scaling).

The D(^{3}He) minority case is much more problematic, and the heating results are generally less efficient than the D(H) case. Typical H factors are at most 1.6 (and often

less). The reason for this is not well understood. One issue is the difficulty of controlling, or measuring the ^{3}He concentration in the typical D plasma. Recent results from Alcator C-Mod indicate that the heating efficiency may be optimized by maintaining a 2–3% minority concentration ratio. At higher concentrations off-axis mode-conversion processes may begin to play a significant role, and at lower concentrations the single pass absorption becomes too low. As pointed out in the Theory Section, in moderate aspect ratio tokamaks such as JET or C-Mod, the shear-Alfvén wave mode conversion layer may provide an undesirable parasitic edge absorption mechanism. At the present time in the D(^{3}He) case a quantitative demonstration of the various absorption processes (i.e., power balance) is not yet available. Furthermore, not even a qualitative demonstration of the SAW MC process is available. Since "seeding" a D–T plasma with a few percent ^{3}He for minority absorption is thought to be important for initial heating in a D-T plasma [8] (and ultimately $2\Omega_T$ would take over at sufficiently high beta), a thorough experimental documentation of power balance with D(^{3}He), including both central (IBW) and edge (SAW) mode conversion processes, is of great importance.

b. Plasma Rotation During ICRF Heating

Impurity toroidal rotation has been measured in JET, TFTR and in Alcator C-Mod during ICRF heating [9,10,11]. The rotation has been deduced from the Doppler shifts of argon x-ray lines in C-Mod. As an example, a typical shot from Alcator C-Mod is shown in Fig. 5. Rotation velocities greater than 1.2×10^7cm/s ($\omega = 200$ kRad/sec) in the co-current direction have been observed in H-mode discharges that had no direct momentum input. The increase in the central impurity rotation velocity was approximately proportional to the increase in the plasma stored energy (confinement enhancement). The toroidal rotation veocity is highest near the magnetic axis, and decreases with increasing minor radius. A radial electric field of 300 V/cm at r/a = 0.3 has been inferred from the force balance equation. The direction of the rotation changed when the plasma current direction was reversed, remaining co-current. Impurity toroidal rotation in ICRF heated plasmas is in the direction opposite to the rotation in ohmic L-mode plasmas; co-current rotation has also been observed during purely ohmic H-modes. When the ICRF heating was turned off, the toroidal rotation decayed with a characteristic time of order 50 ms, similar to the energy confinement time, and much shorter than the calculated neoclassical momentum damping time. This phenomenon is presently not well understood.

c. Harmonic Heating at $2\Omega_D$

Harmonic heating at $\omega = 2\Omega_H$ was carried out earlier on the JT-60U tokamak, and more recently on JET [12] at $2\Omega_H$ and $(2\text{–}3)\Omega_D$. Since the absorption efficiency is proportional to the ion-beta, this is not an efficient scenario for initial plasma heating (for $2\Omega_D$, there is always the Ω_H fundamental minority resonance backup). Recent results may be found in D-T plasmas in JET [13]. We note that in moderate to high field devices ($B \geq 4$ T) the $2\Omega_H$ scenario requires a rather high transmitter frequency ($f \gtrsim 120$ MHz) where power generation becomes less efficient (tube powers decrease to below 1.5 MW). As we shall see below, $2\Omega_D$ absorption in the presence of NBI injection becomes important via the energetic beam deuterons.

d. Mode Conversion Heating Experiments

Direct electron heating and current drive via mode converted ion Bernstein waves using a low field side antenna in a tokamak were first demonstrated in the TFTR device [14]. Mode conversion electron heating (MCEH) experiments were done in gas-puffed plasmas consisting of ^{3}He, ^{4}He, and D, at $B_0 = 4.5$ T, $n_e(0) = 4.0 \times 10^{19}$ m^{-3}, and $I_p = 1.7$ MA. The ICRF transmitters were operated at 43 MHz with a symmetric fast wave power spectrum characterized by $k_{||} \simeq 10$ m^{-1}. Up to 10 keV peak electron temperatures were achieved using 3.3 MW of ICRF power with 3 keV target plasma. The position of the peak in electron heating could be changed by varying the concentration of ^{3}He, in agreement with theory. The full-width at half maximum of the power deposition profile was typically $0.15 - 0.20$ m, as deduced from break in slope measurements of the electron temperature versus time.

More recently, highly localized (FWHM $\simeq 0.2\ a$) on-axis and off-axis electron heating via mode converted ion Bernstein waves (IBW) has been observed in Alcator C-Mod. Direct electron heating from the IBW was measured using a break in slope analysis of the electron temperature versus time, as measured by the grating polychromator (GPC). A state of the art toroidal full-wave ICRF code (TORIC) [15] developed by M. Brambilla has been implemented at MIT and has been used to analyze these mode conversion electron heating experiments. This full-wave model solves explicitly for the mode converted IBW electric field, as well as the electric field of the launched fast wave. An artificial broadening of the ion-ion hybrid resonance layer has been implemented which ensures a well-behaved solution for the electric field near mode conversion. Important effects on wave propagation and absorption such as focussing and diffraction, as well as volumetric effects are naturally included in this model.

The experimental and predicted RF power deposition profiles to electrons for on-axis MCEH in an H(^{3}He) C-Mod plasma are shown in Fig.6. The plasma parameters

were $B_0 = 6.2$ T, $n_e(0) = 1.8 \times 10^{20}$ m^{-3}, $I_p = 0.8$ MA, $P_{RF} = 1.2$ MW, $n_{^3He}/n_e = 0.25$, $n_H/n_e = 0.45$, and $n_D/n_e = 0.05$. The measured and predicted RF deposition profiles agree quite well in shape and magnitude. The integrated RF power fraction to electrons for the predicted profile is $\eta_e^{RF} = 0.91$, while the measured RF power fraction to electrons is $\eta_e^{RF} = 0.79$. The remaining RF power in the simulation is absorbed at the ^{3}He cyclotron resonance ($\eta_{^3He}^{RF} = 0.09$). Calculations carried out with a 1-D full-wave ICRF code (FELICE) [16] for this same case indicate similar absorbed RF power fractions but much lower central RF power densities (by a factor of 10). The lower peak power densities arise from the absence of wave focussing and volumetric effects in the 1-D analysis. The peakedness of the RF power deposition profile was found to be a strong function of the level of background deuterium in the experiment. Theoretical and numerical analysis of this effect indicated that as the level of D increased to $n_D/n_e \gtrsim 0.1$, the wave dispersion changes and the perpendicular damping lengths of the IBW increase because of an increase in the perpendicular group velocity [17,18].

The experimental and predicted RF electron heating profiles for off-axis MCEH in a D(^{3}He) C-Mod plasma are shown in Fig. 7. The plasma parameters were $B_0 = 7.9$ T, $I_p = 1.2$ MA, $n_e(0) = 2.5 \times 10^{20}$ m^{-3}, $n_{^3He}/n_e = 0.30$ and $n_D/n_e = 0.40$. The location of the peak in the predicted power deposition ($r/a \simeq 0.55$) is in reasonably good agreement with experiment. The absorbed rf power fraction to electrons predicted by TORIC is $\eta_e^{RF} = 0.56$, with $\eta_{^3He}^{RF} = 0.44$. This electron absorption is close to the experimentally deduced value of $\eta_e^{RF} \simeq 0.50$.

Electron heating by mode conversion has also been observed on ASDEX-U, and the power deposition profile was measured by modulation techniques using a 45 channel ECE system, as well as with break-of-slope techniques [19].

e. Mode Conversion Current Drive

Mode conversion current drive (MCCD) experiments were performed in TFTR [14] by operating the fast wave antenna with co- and counter- phasing ($k_\parallel \simeq 6$ m^{-1}). Up to 130 kA of RF current was driven with 2.2 MW of ICRF power at $T_e(0) \sim 7$ keV. The corresponding current drive figure of merit for this case was $\eta_{cd} \simeq 0.07$ (10^{20} A/W/m^2), in good agreement with the theoretical values are based on a combined 1-D calculation of the IBW power deposition to electrons (FELICE code) and the Ehst-Karney formulation of the current drive efficiency [5]. In these experiments $Q \simeq 0.1$ in Eq.(11), a rather high value.

To calculate current drive efficiency, the full-wave TORIC code has been combined with an adjoint calculation [5] of the current drive efficiency. The combined model is valid for driven current via fast magnetosonic waves or mode converted IBW. This model

has been used to assess possible current profile control experiments in D(^{3}He) plasmas in Alcator C-Mod. One possible on-axis mode conversion current drive (MCCD) scenario is shown in Fig. 8. The parameters used in this case were $f_0 = 43$ MHz, $B_0 = 5.0$ T, $n_e(0) = 1.5 \times 10^{20}$ m^{-3}, $T_e(0) = 3.0$ keV, $n_\phi = 5$ ($k_{\parallel_{ANT}} \simeq 5.4$ m^{-1}), $n_{^3He}/n_e = 0.25$, and $n_D/n_e = 0.50$. The normalized phase speed of the injected waves near the mode conversion layer is $v_\parallel/v_{te} \simeq 1.0$ and the driven current is $I_{MCCD} \simeq 100$ kA, assuming 3 MW of incident ICRF power. The resulting current drive figure of merit is $\eta_{cd} \simeq 0.027$ (10^{20} A/W/m^2), where $\eta_{cd} = \langle n_e \rangle (10^{20}$ m$^{-3}) I_{RF}(kA) R_0(m)/P_{RF}(W). The on-axis RF current density in Fig. 8 is comparable to the ohmic current density at about 1 MA of total current. Thus, significant local modification of the ohmic current density profile would be expected in this case.

An example of off-axis MCCD is shown in Fig. 9. The parameters used in this case were were $f_0 = 43$ MHz, $B_0 = 4.19$ T, $n_e(0) = 1.5 \times 10^{20}$ m^{-3}, $T_e(0) = 3.0$ keV, $n_\phi = 5$ ($k_{\parallel_{ANT}} \simeq 5.4$ m^{-1}), $n_{^3He}/n_e = 0.25$, and $n_D/n_e = 0.50$. The normalized phase speed of the injected waves near the mode conversion layer [$(r/a)_{mc} \simeq 0.5$] is $v_\parallel/v_{te} \simeq 0.97$ and the driven current is $I_{MCCD} \simeq 60 - 70$ kA, assuming 3 MW of injected ICRF power. The resulting current drive figure of merit is $\eta_{cd} \simeq 0.019$ (10^{20} A/W/m^2). Again, the local driven current density near the mode conversion layer is comparable to the local ohmic current density at that point.

f. Fast Wave Electron Heating and Current Drive

Initial experiments on DIII–D showed effective central electron heating [20] and current drive [21,22] with fast waves, and achieved full non-inductive current drive, in combination with ECH, using a single fast wave antenna [23]. The good heating results were obtained in spite of the relatively low single pass efficiency ($A \sim 5-20\%$), implying efficient multiple pass absorption. For single pass absorption of less than 4% the central heating and current drive efficiency deteriorated rapidly in DIII-D. More recently, the FWCD system has been extended by adding two 2 MW transmitters that have a frequency range of 30–120 MHz and two four-strap antennas to the existing four-strap antenna and 2 MW, 30–60 MHz transmitter. For the experiments reported in this paper, one antenna was tuned to 60 MHz while the other two antennas were operated at 83 MHz; these frequencies correspond to 4–7 times the deuterium cyclotron frequency.

Recent experiments on DIII–D have studied the physics of FWCD in a neutral beam injection (NBI) environment. All of the advanced tokamak scenarios proposed for DIII–D utilize NBI heating as well as RF heating, and many of the critical diagnostics on DIII–D such as the motional Stark effect (MSE) and charge exchange recombination (CER) emission require the NBI system. During these current drive experiments, the partial absorption of the fast waves by energetic beam ions at high harmonics of the ion cyclotron

frequency was also studied; this interaction is a major issue for low aspect ratio tokamaks such as NSTX, where a combination of NBI and FWCD may be used simultaneously.

Measurements of the radial profile of the fast wave driven current in non-sawtoothing discharges on DIII–D, formed by early NBI during the plasma current ramp-up, allows a stringent comparison between theory and experiment. From a time sequence of magnetic equilibrium reconstructions using the MSE data, the profiles of toroidal electric field and total current density were determined; the non-inductive current density was then found by subtracting the inductive current density from the total current density assuming neoclassical resistivity [24]. The FWCD radial profile was found from the change in the non-inductive current profile as the antenna phasing was changed from co to counter current drive under otherwise similar conditions. The FWCD radial profile determined with this method is shown in Fig. 10 for a L-mode plasma with 280 kA of integrated FWCD. This figure also shows the theoretical predictions from 3 models: the FASTCD model based on the ergodic, weak damping limit [25], the CURRAY ray-tracing model that includes multiple reflections [26], and the PICES reduced full-wave model [27]. The measured fast wave driven current is highly localized on axis and is in good agreement with theoretical models, as found previously on DIII–D. The integrated non-inductive currents from the 3 models all come within 10% of the measured value.

The important experimental verification of theory is that the measured FWCD efficiency was observed to increase linearly with the electron temperature. This is shown in Fig. 11, where the $B_T = 1$ T data were derived from a surface loop voltage analysis [21,22] and the $B_T = 2$ T data were derived from co/counter comparisons of the non-inductive current profiles as in Fig. 10. The calculated first pass absorption for the points in Fig. 11 ranges typically from 9% to 13%. The predicted scaling of the FWCD efficiency from the CURRAY code, indicated in Fig. 11 by the shaded band, is found to agree with the experiments. This linear electron temperature dependence projects to attractive values for the FWCD efficiency under reactor conditions (i.e, $n_{20} I_{MA} R_M / P_{\rm MW} \sim 0.08 T_{e10}$, where the density is measured in units of $10^{20}\mathrm{m}^{-3}$, I in MA, R in m, P in MW, and $T_e(0)$ in units of 10 keV). Results from Tore–Supra [28] are also indicated on this figure, in good agreement with theoretical predictions.

g. <u>High Cyclotron Harmonic Absorption on Beam Ions</u>

The interaction of fast waves with energetic beam ions at high harmonics of the ion cyclotron frequency was studied in parallel with the current drive experiments in DIII-D. The partial absorption of fast waves by beam ions was evident from a build up of fast particle pressure near the magnetic axis (resulting in an increased Shafranov shift) and a correlated increase in the neutron rate. The anomalous fast ion stored energy could be as much as a quarter of the stored energy in the plasma, and the anomalous neutron rate

could be half of the total neutron rate. The anomalous neutron rate, $\Delta S_n = S_n - S_{calc}$, and anomalous fast ion stored energy, $\Delta W = W_{tot} - W_{th} - W_{beam}$, peaked when a harmonic of the deuterium cyclotron frequency passed through the center of the plasma, as shown in Fig. 12 for a L-mode magnetic field scan at constant auxiliary power and safety factor. The anomalous neutron rate and stored energy built up during the fast wave pulse over several tenths of a second, which is the source of the spread in ΔS_n and ΔW in Fig. 12. The largest values of ΔS_n were obtained when the 6th and 7th harmonics of the deuterium cyclotron frequency for the main FWCD frequency of 83 MHz passed through the axis of the plasma. The value of ΔW also peaked at the $6\Omega_D$ resonance and showed a small increase at the $7\Omega_D$ resonance as well. A simple estimate of the fast wave power absorbed by the beam ions can be made from $P_{abs} \approx \Delta W/\tau_s$, where τ_s is the slowing down time of the ion tail. For the case in Fig. 12 where the $6\Omega_D$ resonance passed through the plasma center, this estimate gives $P_{abs}/P_{fw} \sim 0.3$ using a calculated value of $\tau_s \approx 0.2$ sec for the plasma center.

The partial absorption of fast waves by beam ions appears to decrease the experimental FWCD efficiency. The measured FWCD efficiency, normalized to the central electron temperature, is shown in Fig. 13 as a function of the magnetic field strength; the theoretical efficiency assuming no ion absorption is also plotted for comparison. For $B_T \geq 2$ T, where the interaction between the fast waves and the beam ions was weakest, the measured FWCD efficiency was in good agreement with the maximum efficiency that could be theoretically expected. However, as B_T was lowered, the experimental FWCD decreased to approximately half of the maximum theoretical value. This reduction in the FWCD efficiency is likely due to beam ion absorption of the fast waves, which would reduce the amount of power available for current drive. Equation (8) has been used for estimating the ICRF power absorption by a diffused beam ion model. Initial estimates are in reasonable agreement with experimental observations.

h. Advanced Modes of Operation with ICRF

There are several advanced modes of operation with ICRF heating, usually in combination with some other technique to control the central particle source (PEP mode), edge radiating mantle (RI mode), or current profile (optimized shear, or OS mode). We shall discuss some of these experimental results briefly here.

(a) Pellet Enhanced Mode (PEP)

This mode was originally discovered in JET [9], and further studied in Alcator C-Mod [6]. The good confinement regime is obtained when a pellet is injected into the plasma, followed by intense central ICRF heating (either the H or He-3 minority technique). After an initial cooling of the plasma, rapid reheating occurs, with excellent confinement in the

core of the plasma column, typically at radii r/a $\leq$ 0.3, where the density and plasma pressure strongly peak. By injecting a second Li pellet and observing the angle of the ablation cloud relative to the magnetic field, the the q-profile could be determined. It was found that a reversed shear equilibrium was present, with q_{min} at r/a=0.3. Within the reversed shear region the pressure strongly peaked, and the transport was reduced to neoclassical values. This mode of operation is then similar to negative central shear (NCS) or reversed shear (RS) or optimized shear (OS) mode of operation regimes with NBI central heating and fuelling. Unfortunately the PEP mode is transient, and it collapses after a short time, apparently either due to beta-limit, or due to a diffusion of the bootstrap current generated by the peaked pressure profile (not yet understood). Future experiments might include driving off-axis currents to replace the bootstrap current near q_{min}, hence extending the PEP mode toward quasi-steady state.

(b) Radiative Improved Mode

This mode of operation was observed in the TEXTOR experiment [29]. By seeding the plasma with neon (or other inert gas) a radiating edge mantle was created (as much as 80-90% of the power was radiated from the edge) but with acceptable core radiation. Good confinement scaling was obtained and the confinement follows the neo-Alcator type of scaling even at densities close to the Greenwald limit (see Fig. 14). In particular, an H factor equal to ITER 93H scaling was obtained. This mode of operation does not require a divertor, and the local heat load on the first wall of a reactor would be minimized. This is a quasi-steady state mode of operation, hence reactor relevant. Issues include extrapolation to large machines, and keeping Zeff at or below 1.6, as required in a working fusion reactor. The good confinement is obtained only if 25% or more of the heating power is in the form of Co-NBI (the remaining can be ICRF or counter-NBI or co+counter-NBI). Perhaps central fueling is again important, just like for the PEP mode.

(c) Hot Ion H-Mode with Optimized Shear

The highest performance (neutron rate) in JET in a DD plasma has been obtained with ICRF central heating with current ramp (reversed shear, or optimized shear) and neutral beam heating [12,13]. An example of this technique is shown in Fig. 15. This case corresponds to D(H) minority heating (electrons) and $2\omega_D$ harmonic cyclotron absorption by the beam ions (ion heating). Record neutron rates have been obtained by this technique in DD plasmas (a neutron rate of 6×10^{16} neutrons/sec. This regime shows the combined effectiveness of electron and ion heating with ICRF techniques.

IV. Summary

Heating and current drive with RF waves in the ion cyclotron range of frequencies (ICRF) has been found to be a highly effective means to control plasma parameters in

present day tokamaks. In this paper we have summarized the basic theoretical predictions and presented some of the most recent experimental results in their support. We have found that heating in deuterium plasmas with hydrogen minority, or the D(H) scenario, is very effective in tokamaks of all sizes, and that high quality H-modes are readily obtained. Owing to the lower single pass absorption, heating with the D(He-3) scenario is not quite as efficient, and lower H-factors are obtained. The underlying physics is not well understood at the present time. Possible competing edge absorption mechanisms have been identified in the paper. This is an area where more work needs to be done, especially since this may be a startup scenario in D-T plasmas before second harmonic tritium absorption takes over at sufficiently high ion betas.

We have also discussed cyclotron harmonic absorption results, and indicated that second harmonic absorption on the majority deuterium component may also be important. Furthermore, higher cyclotron harmonic absorption of the fast wave on fast beam ions has been observed. This has to be understood better since FW current drive at higher cyclotron harmonics has been shown to be an effective means of central RF current drive, at least in the absence of a fast ion population. These results are of particular importance when we consider applications in a burning plasma with a significant alpha particle population. In the absence of beam ions, direct fast wave electron heating and current drive has been thoroughly demonstrated, and the linear dependence of current drive efficiency on electron temperature, as well as the radial variation of current profile has been documented.

Another important area of progress is electron heating and current drive associated with the mode-converted ion Bernstein waves (IBW). On-axis heating and current drive for favourable conditions has been found to be efficient in a few experimental tries. However, off-axis heating and current drive is still not well documented. This technique needs more attention since profile control is of major importance in improving tokamak performance, and MCCD with IBW is one of the more promising techniques. Similarly, formation of ion and electron thermal barriers (ITB, ETB) using the concept of RF shear-flow will have to be developed further, both theoretically and experimentally. Plasma rotation in the presence of minority heating may be a manifestation of such physical phenomenon, although this idea has not been explored yet in any depth. Another promising technique in this direction is direct IBW launch. We have not had space to discuss this promising technique in this paper, neither have we had space to discuss the control of MHD phenomena using ICRF waves. Along these lines, it is important to note the formation of improved tokamak performance by ICRF techniques in combination with particle fuelling. Noteworthy regimes are the optimized shear (OS) scenario, the PEP mode (where central fuelling with pellet injection is combined with ICRF heating) and the RI mode, where edge fuelling with neon gas, combined with NBI and ICRF heating (50-50%) leads to edge thermal barrier

formation and effective power dissipation by edge radiation, while retaining excellent core confinement. Clearly, in the future further work is needed in this area.

Acknowledgements

This work was supported by DOE Contract No.DE-AC02-78ET51013.

References

[1] T.H. Stix, Waves in Plasmas, (Am. Institute of Physics, New York, NY, 1992).

[2] M. Porkolab in Advances in Plasma Physics, AIP Conf Proceedings **314** (Am. Institute of Physics, New York, NY, 1994, Ed. N.J. Fisch) 99.

[3] A. Ram, A. Bers, S.D. Schultz and V. Fuchs, Phys. Plasmas **3**, (1996) 1976.

[4] N.J. Fisch, Rev. Modern Physics, **59**, (1987) 175.

[5] D.A. Ehst and C.F.F. Karney, Nucl. Fusion **31**, (1991) 1933.

[6] Y. Takase, R.L. Boivin, F. Bombarda, P.T. Bonoli, C. Christensen, C. Fiore, D. Garnier, J.A. Goetz, S.N. Golovoto, R. Graneta, M. Greenwald, S.F. Home, A. Mazurenko. G. McCracken, P. O'Shea, M. Porkolab, J. Reardon, J. Rice, C. Rost, J. Schachter, J.A. Snipes, P. Stek, J. Terry, R. Watterson, B. Welch, and S. Wolfe, Phys. Plasmas **4**, (1997) 1647.

[7] JET ICRF Results: D. Start et al., at this Conference.

[8] V.P. Bhatnagar et al., Proc. of this Conference, p.29.

[9] L.-G. Eriksson, R. Giannella, T. Hellsten et al., Plasma Phys. Control. Fusion **34** (1992) 863; L.-G. Eriksson, E. Righi, K.D. Zastrow, ibid, **39**, (1997) 27.

[10] C.K. Phillips, J. Hosea, E. Marmar, M.W. Phillips, J. Snipes et al, "Ion cyclotron range of frequencies stabilization of sawteeth on Tokamak Fusion Test Reactor", Phys. Fluids B4 (1992) 2155; H. Hsuan, M. Bitter, C.K. Phillips, J.R. Wilson, C. Bush, H.H. Duong, D. Darrow, G.W. Hammett, K.W. Hill, R.P. Majeski, S. Medley, M. Petrov, E. Synakowski, M. Zarnstorff, and S. Zweben, "ICH-induced Plasma Rotation on TFTR", Radio Frequency Power in Plasmas, AIP Conf. Proceedings **355** Palm Springs, CA, May 1995 (Am. Institute of Physics, New York, NY, 1996, Eds. R. Prater, V.S. Chan) 39.

[11] J.E. Rice, M. Greenwald, I.H. Hutchinson, E.S. Marmar, Y. Takase, S.M. Wolfe, F. Bombarda, Nuclear Fusion **38**, (1998) 75.

[12] M. Mantsinen, V. Bhatnagar, J. Carlsson, G.Cottrell, L.-G. Eriksson, A. Gondhalekar, C. Gormezano, T. Hellsten, R. König, P. Lomas, E. Righi, F. Rimini, G. Sips, D. Start, F.X. Söldner, B. Tubbing and K.-D. Zastrow, 24*th* EPS Conf. on Contr. Fusion and

Plasma Physics, Berchtesgaden, Germany, June 9–13, 1997, Vol.21A, Part I, pp.137.

[13] D.F.H. Start, V. Bergeaud, L.G. Eriksson, B. Gayral, C. Gormezano and M. Mantsinen, 24*th* EPS Conf. on Contr. Fusion and Plasma Physics, Berchtesgaden, Germany, June 9–13, 1997, Vol.21A, Part I, pp.141.

[14] R. Majeski, J.H. Rogers, S.H. Batha, R. Budny, E. Rredrickson, B. Grek, K. Hill, J.C. Hosea, B. LeBlanc, F. Levinton, M. Murakami, C.K. Phillips, A.T. Ramsey, G. Schilling. G. Taylor, J.R. Wilson adn M.C. Zarnstorff, Phys. Rev. Lett. **76** (1996) 764.

[15] M. Brambilla, "A full-wave code for ion cyclotron waves in toroidal plasmas", IPP Report 5/66, Garching (February, 1996).

[16] M. Brambilla, Nucl. Fusion **28** (1988), 549.

[17] P.T. Bonoli, P. O'Shea, M. Brambilla et al., Phys. Plasmas **4** (1997), 1774.

[18] P.J. O'Shea, P. Bonoli, A. Hubbard, M. Porkolab, and Y. Takase, Proc. of 12^{th} Topical Conf. on Radio Frequency Power in Plasmas, eds, P.M. Ryan and T. Intrator, AIP Conf. Proc. 403, (AIP, New York, 1997), p. 89.

[19] J.M. Noterdaeme, S. Wukitch, D.A. Hartman et al., in Proc. Sixteenth IAEA Fusion Energy Conference, Montreal, Canada, 7-11 October 1996, IAEA-CN-64/F1-EP-4.

[20] C.C. Petty, R.I. Pinsker, M. Mayberry et al., Phys. Rev. Lett. **69**, (1992) 289.

[21] R. Prater, R.A. James, C.C. Petty et al., Plasma Phys. Control. Fusion **35**, (1993) A53.

[22] R.I. Pinsker, C.C. Petty, M. Porkolab et al., in Plasma Physics and Controlled Nuclear Fusion Research (Proc. 14th Int. Conf. Würzburg, 1992), Vol. 1, p. 683.

[23] C.C. Petty, R. Pinsker, M.E. Auston et al., Nucl. Fusion **35**, (1995) 773.

[24] C.B. Forest, K. Kaufer, T.C. Luce, P.A. Politzer et al., Phys. Rev. Lett. **73**, (1994) 2444.

[25] K. Kupfer, C.B. Forest, C.C. Petty, and R.I. Pinsker, Phys. Plasmas **1**,(1994) 3915 .

[26] T.K. Mau, S.C. Chiu, R.W. Harvey et al., in Radiofrequency Heating and Current Drive of Fusion Devices (Proc. 19^{th} Eur. Conf. Brussels, 1992), Vol. 16E, p. 181.

[27] E.F. Jaeger, D.B. Batchelor, D.C. Stallings et al., Nucl. Fusion **33**, (1993) 179.

[28] A. Becoulet, Plasma Physics and Controlled Fusion **38** (1996) A1.

[29] B. Unterberg, A.M. Messiaen, J. Ongena, M. Brix, G. Bertschinger, J. Boedo, G. Bonheure, M. Ciotti, Th. Denner, F. Durodie, P. Dumortier, K.H. Finken, G. Fuchs,

R. Jaspers, Y.M. Kim, R. Koch, L. Könen, H.R. Koslowski, A. Krämer-Flecken, A. Lyssoivan, G. Mank, G. Van Oost, A. Pospiezczyk, V. Philipps, J. Rapp, U. Samm, B. Schweer, G. Telesca, M.Z. Tokar, R. Uhlemann, P.E. Vandenplas, M. Vervier, G. Waidmann, G. Van Wassenhove, F. Weschenfelder, R.R Weynants and G.H. Wolf, Plasma Phys. Control. Fusion **39** (1997) B189.

Figure Captions

Fig 1: D(H) minority resonance case at 5.3 T and 80 MHz in Alcator C-Mod. R= 0.67 m, a = 0.22 m. The antenna surface is at R = 0.92 m.

Fig. 2: D(^{3}He) minority resonance case at 7.9 T and 80 MHz in Alcator C-Mod. R = 0.67 m, a = 0.22 m. The antenna surface is at R = 0.92 m.

Fig. 3: Typical Alcator C-Mod RF shot, resulting in enhanced D_α confinement with H = 2× ITER 89P. B = 5.3 T, I_p = 1.0 MA, D(H) case.

Fig. 4: D(H) minority heating with ICRF power in JET, as compared with NBI heating. I_p = 2.6 MA, B= 2.6 T, 42 MHz.

Fig. 5: The time histories of several parameters in Alcator C-Mod for a 5.3 T, deuterium H-mode discharge, showing toroidal plasma rotation. In the third frame (c) we show the central electron temperature (with sawteeth) and the central ion temperature (smooth).

Fig. 6: On-axis MCEH in an H(^{3}He) C-Mod plasma. RF electron heating from break in slope analysis compared with predictions of TORIC code.

Fig. 7: Off-axis MCEH in a D(^{3}He) C-Mod plasma. RF electron heating from break in slope analysis compared with predictions of TORIC code.

Fig. 8: On-axis MCCD in an D(^{3}He) C-Mod plasma (f_0 = 43 MHz, B_0 = 5.0 T).

Fig. 9: Off-axis MCCD in a D(^{3}He) C-Mod plasma (f_0 = 43 MHz, B_0 = 4.19 T).

Fig. 10: Radial profile of the non-inductive current density driven by fast waves in DIII-D along with theoretical profiles (B_r = 2.1 T, $\bar{n} = 2.1 \times 10^{19}\mathrm{m}^{-3}$, P_{fw} = 2.1 MW).

Fig. 11: Experimental FWCD efficiency as a function of central electron temperature in DIII-D. The shaded band indicates the predictions from the CURRAY ray tracing code. The solid triangle represents data from Tore-Supra [Ref. 28].

Fig. 12: Toroidal magnetic field dependence of the (a) anomalous neutron rate and (b) anomalous fast ion stored energy ($P_{NI} \approx$ 3.7 MW, $P_{FW} \simeq$ 2.3 MW).

Fig. 13: Toroidal magnetic field dependence of the FWCD efficiency normalized to the central electron temperature.

Fig. 14: RI mode in Textor with neon seeding. I_p = 0.4 MA, B = 2.25 T, shot = 68825.

Fig. 15: Optimized shear mode in JET with NBI and ICRF.

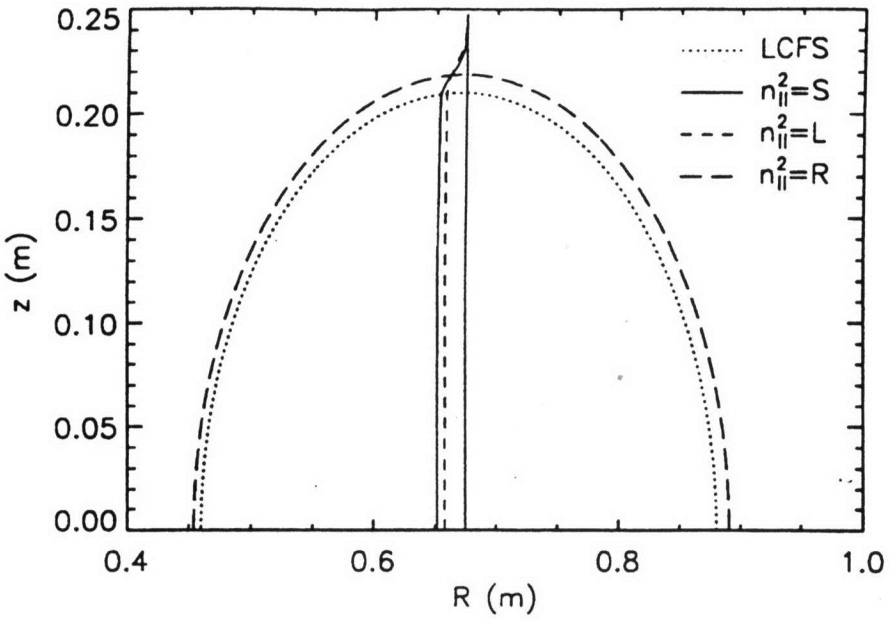

Figure 1: D(H) minority resonance case at 5.3 T and 80 MHz in Alcator C-Mod. R=0.67 m, a = 0.22 m. The antenna surface is at R = 0.92 m. The solid vertical line at R=0.67 m corresponds to the Ω_H resonance.

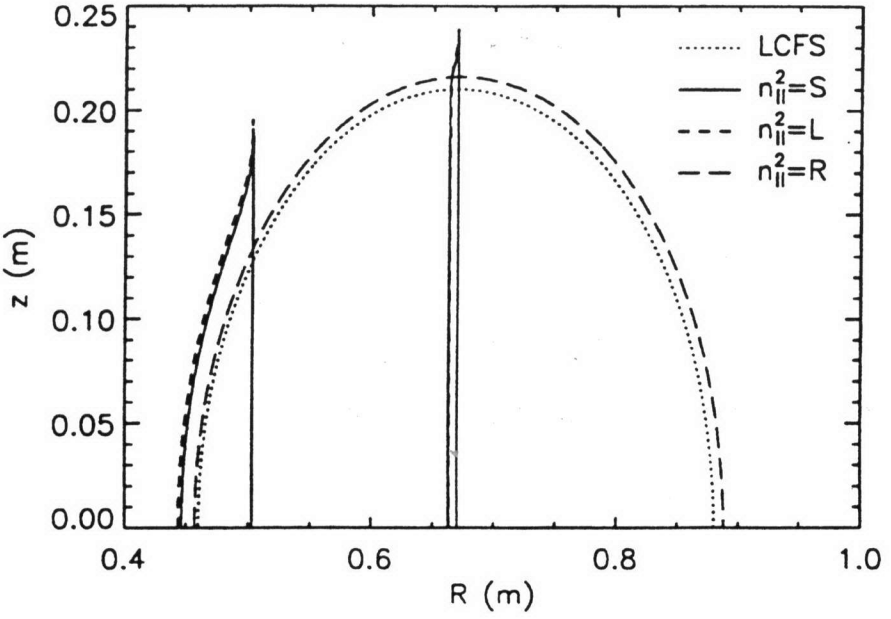

Figure 2: D(^{3}He) minority resonance case at 7.9 T and 80 MHz in Alcator C-Mod. R = 0.67 m, a = 0.22 m. The antenna surface is at R = 0.92 m. The solid line at R = 0.51 m corresponds to the Ω_D resonance and at R=0.67 m is the $\Omega_{^3He}$ resonance.

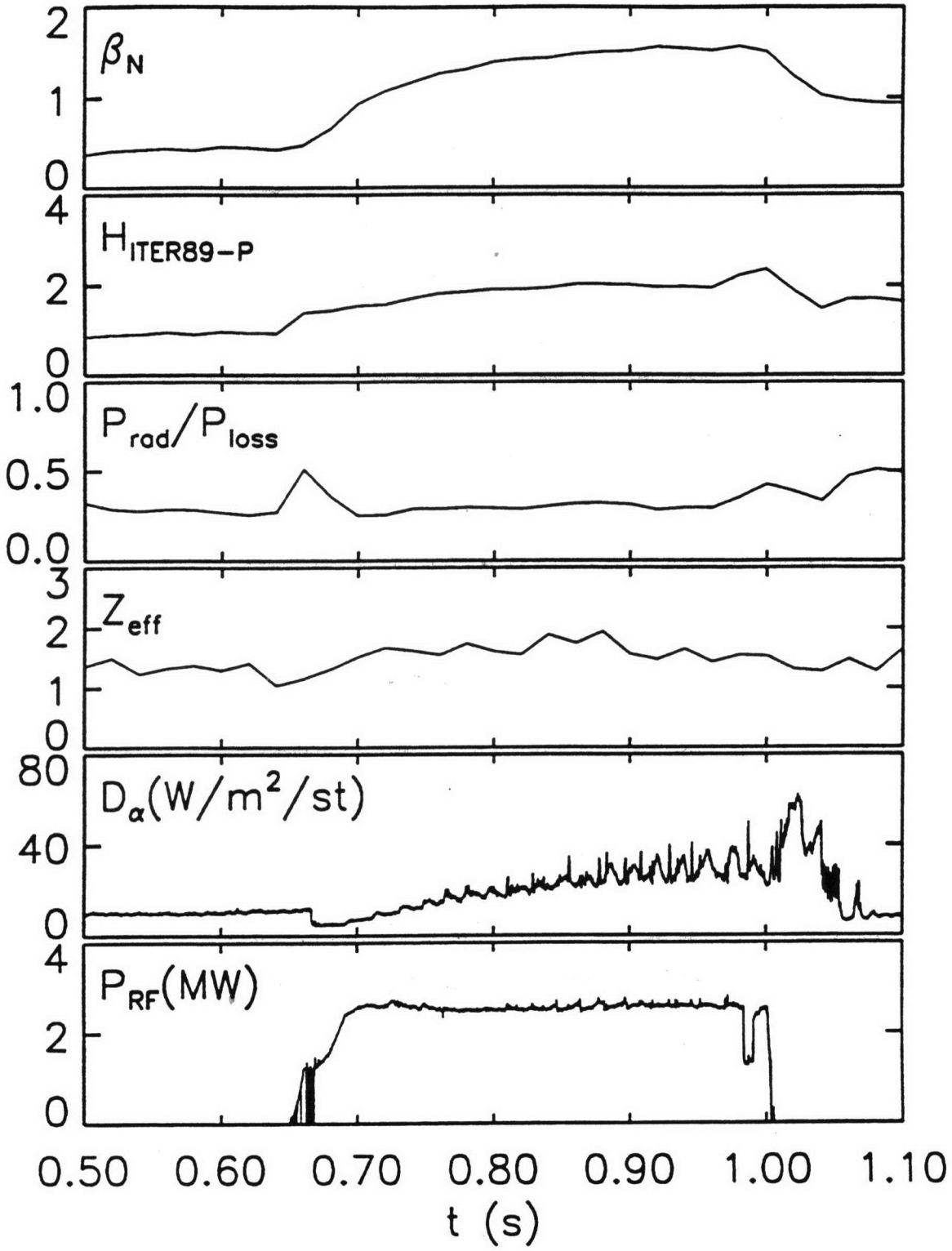

Figure 3: Typical Alcator C-Mod RF shot, resulting in enhanced D_α confinement with H = 2× ITER 89P. B = 5.3 T, I_p = 1.0 MA, D(H) case. Shot = 960116027

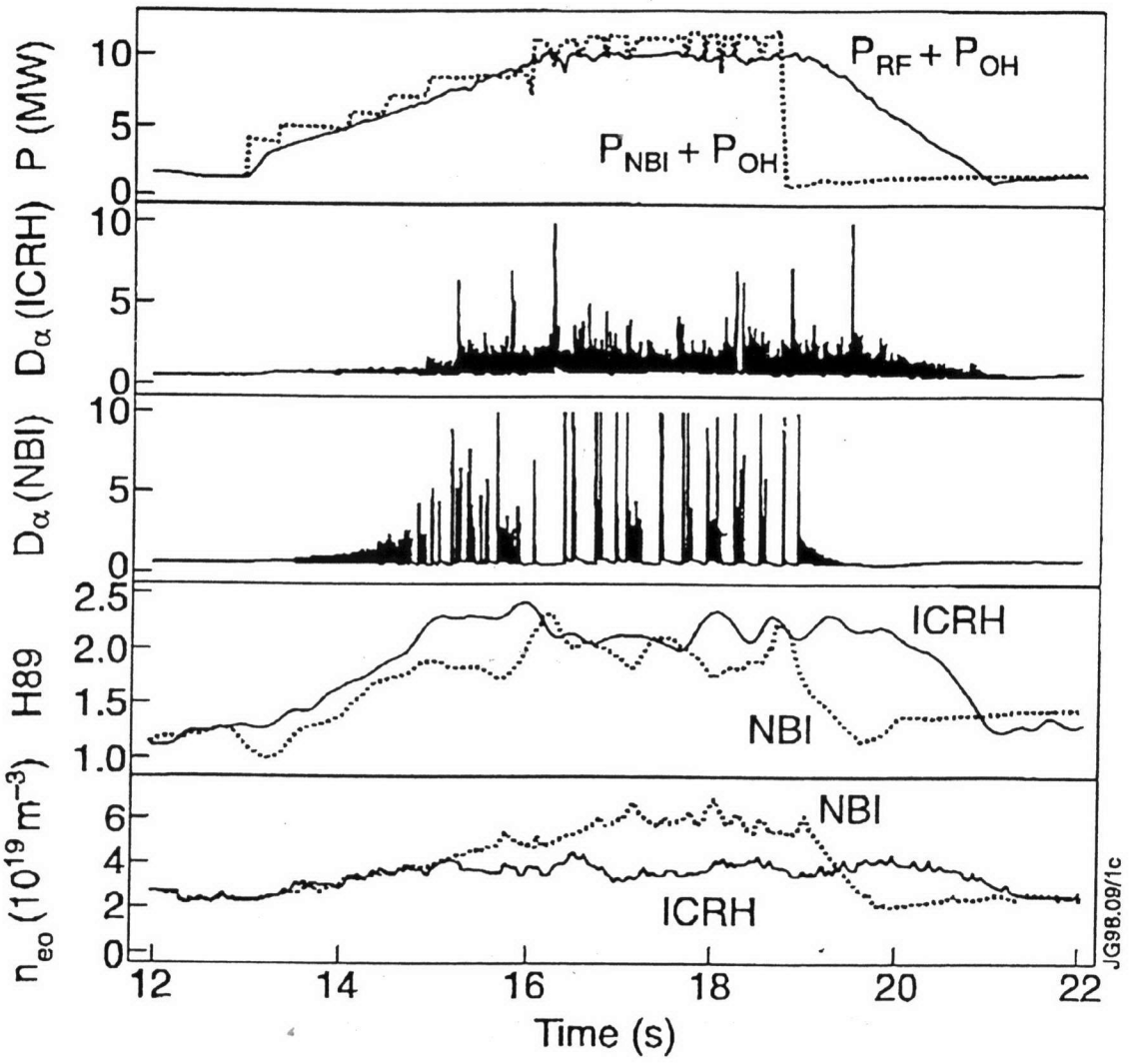

Figure 4: D(H) minority heating with ICRF power in JET, as compared with NBI heating. $I_p = 2.6$ MA, B= 2.6 T, 42 MHz.

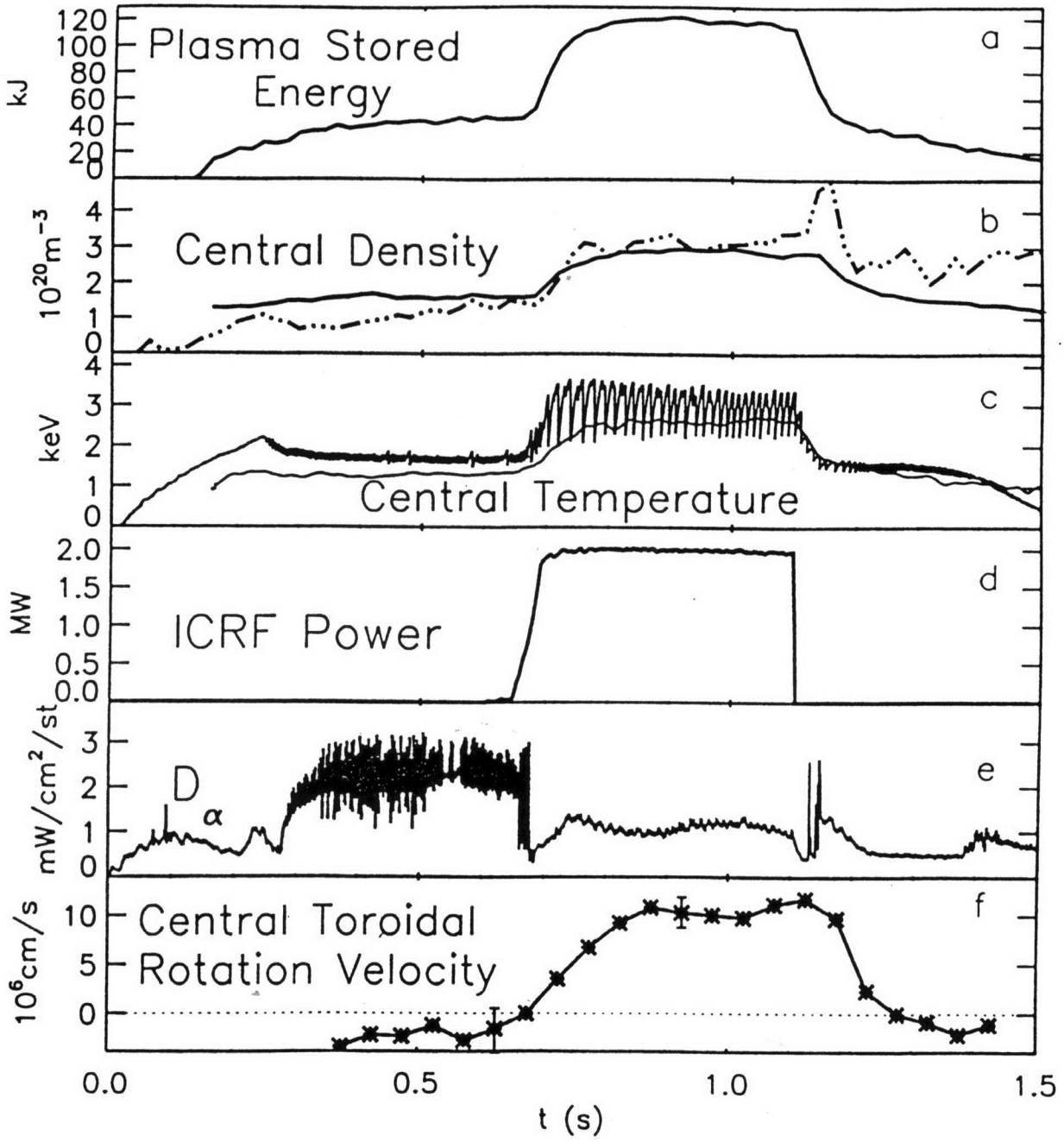

Fig. 5: The time histories of several parameters in Alcator C-Mod for a 5.3 T, deuterium H-mode discharge, showing toroidal plasma rotation. In the third frame (c) we show the central electron temperature (with sawteeth) and the central ion temperature (smooth).

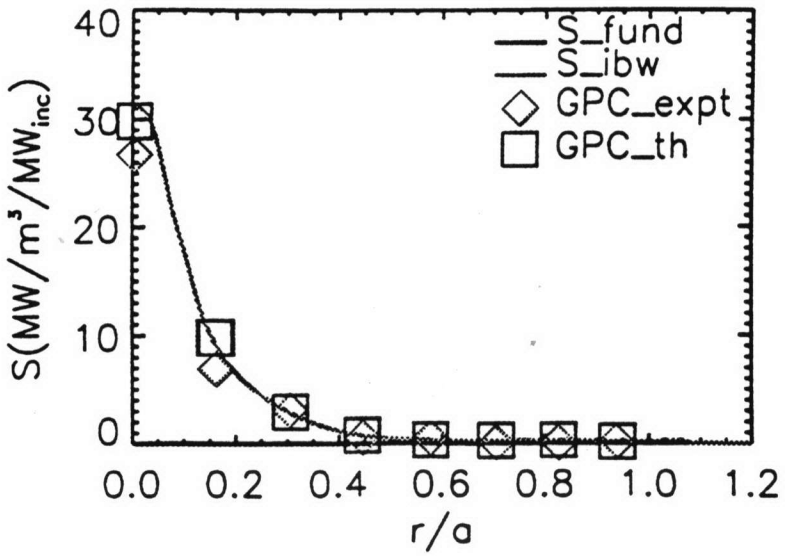

Figure 6: On-axis MCEH in an H(^{3}He) C-Mod plasma. RF electron heating from break in slope analysis compared with predictions of TORIC code.

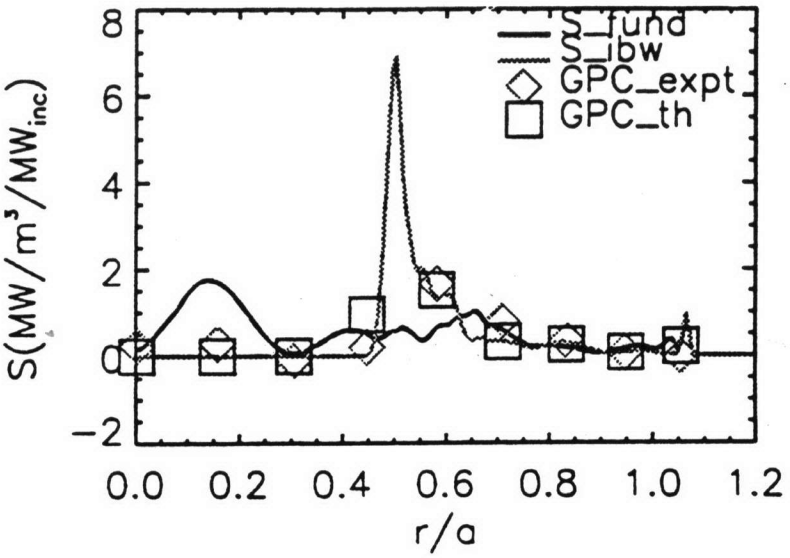

Figure 7: Off-axis MCEH in a D(^{3}He) C-Mod plasma. RF electron heating from break in slope analysis compared with predictions of TORIC code.

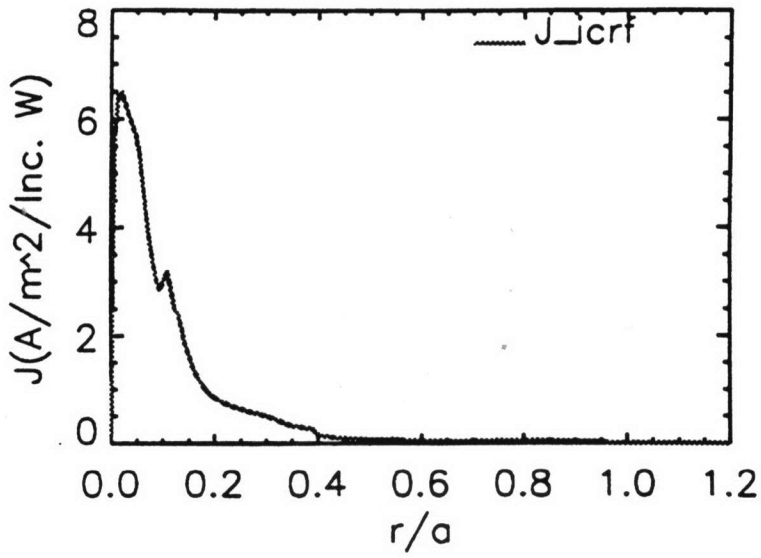

Figure 8: On-axis MCCD in an D(^{3}He) C-Mod plasma ($f_0 = 43$ MHz, $B_0 = 5.0$ T).

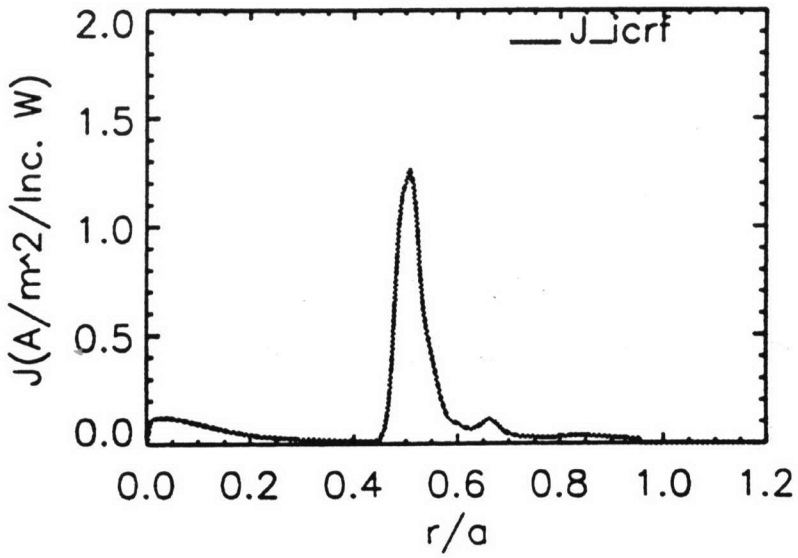

Figure 9: Off-axis MCCD in a D(^{3}He) C-Mod plasma ($f_0 = 43$ MHz, $B_0 = 4.19$ T).

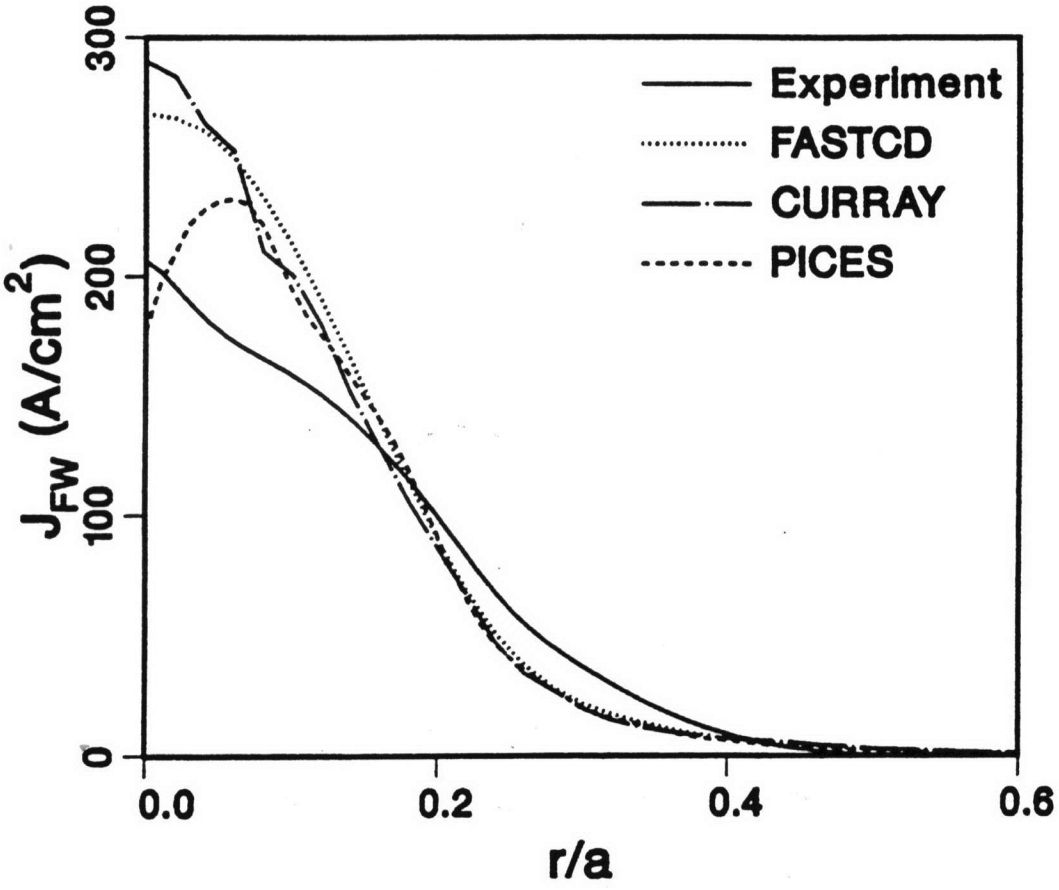

Figure 10: Radial profile of the non-inductive current density driven by fast waves in DIII-D along with theoretical profiles (B_T = 2.1 T, $\bar{n}$ = $2.1 \times 10^{19}\mathrm{m}^{-3}$, P_{NBI} = 5.0 MW, P_{FW} = 2.1 MW).

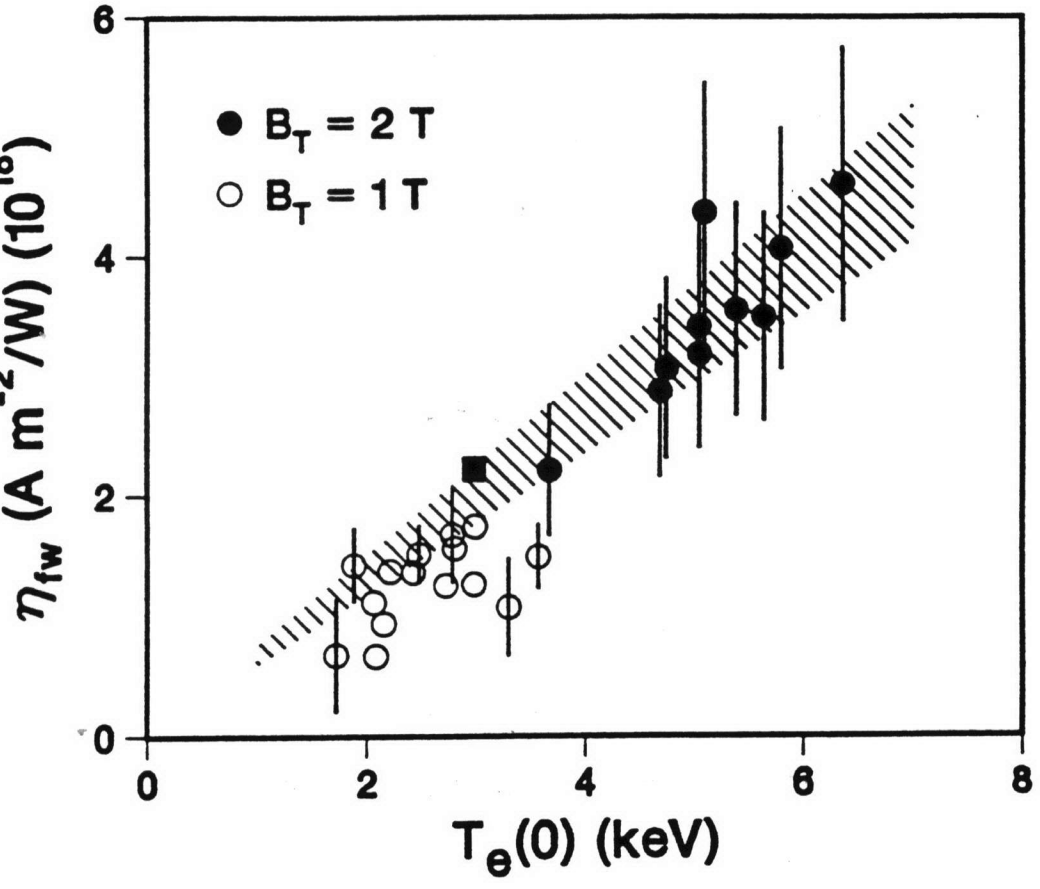

Figure 11: Experimental FWCD efficiency as a function of central electron temperature in DIII-D. The shaded band indicates the predictions from the CURRAY ray tracing code. The solid square represents data from Tore-Supra. [Ref. 28]

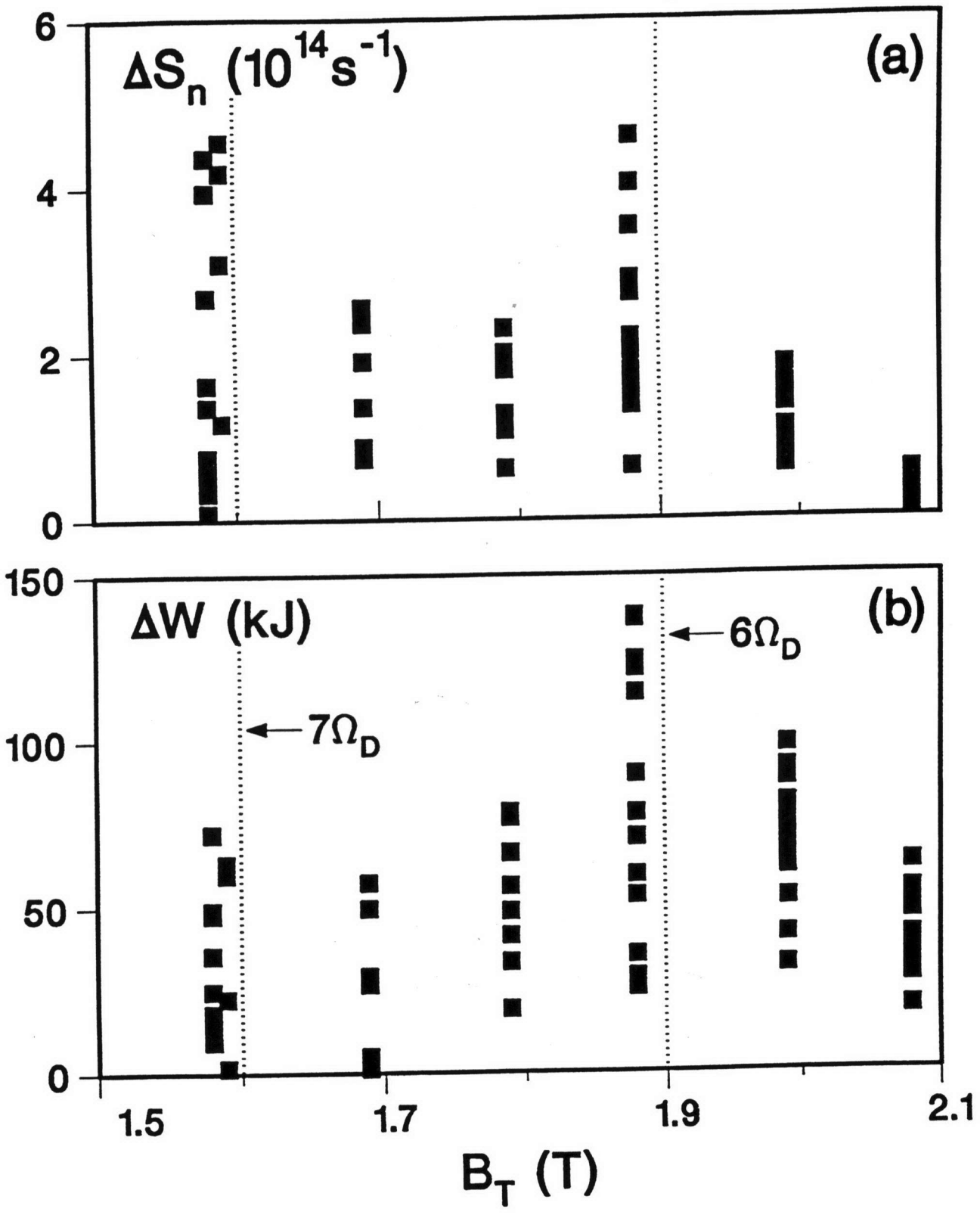

Fig. 12: Toroidal magnetic field dependence of the (a) anomalous neutron rate and (b) anomalous fast ion stored energy ($P_{NI} \approx 3.7$ MW, $P_{FW} \simeq 2.3$ MW).

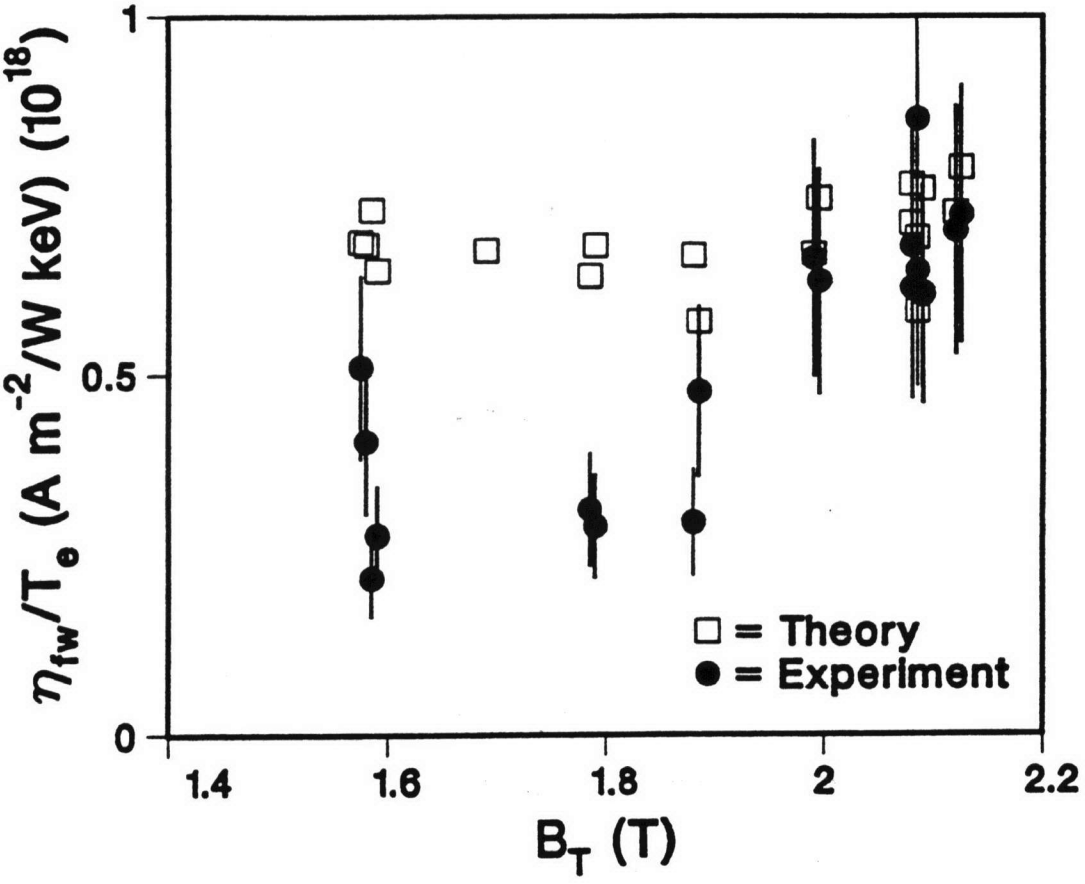

Figure 13: Toroidal magnetic field dependence of the FWCD efficiency normalized to the central electron temperature.

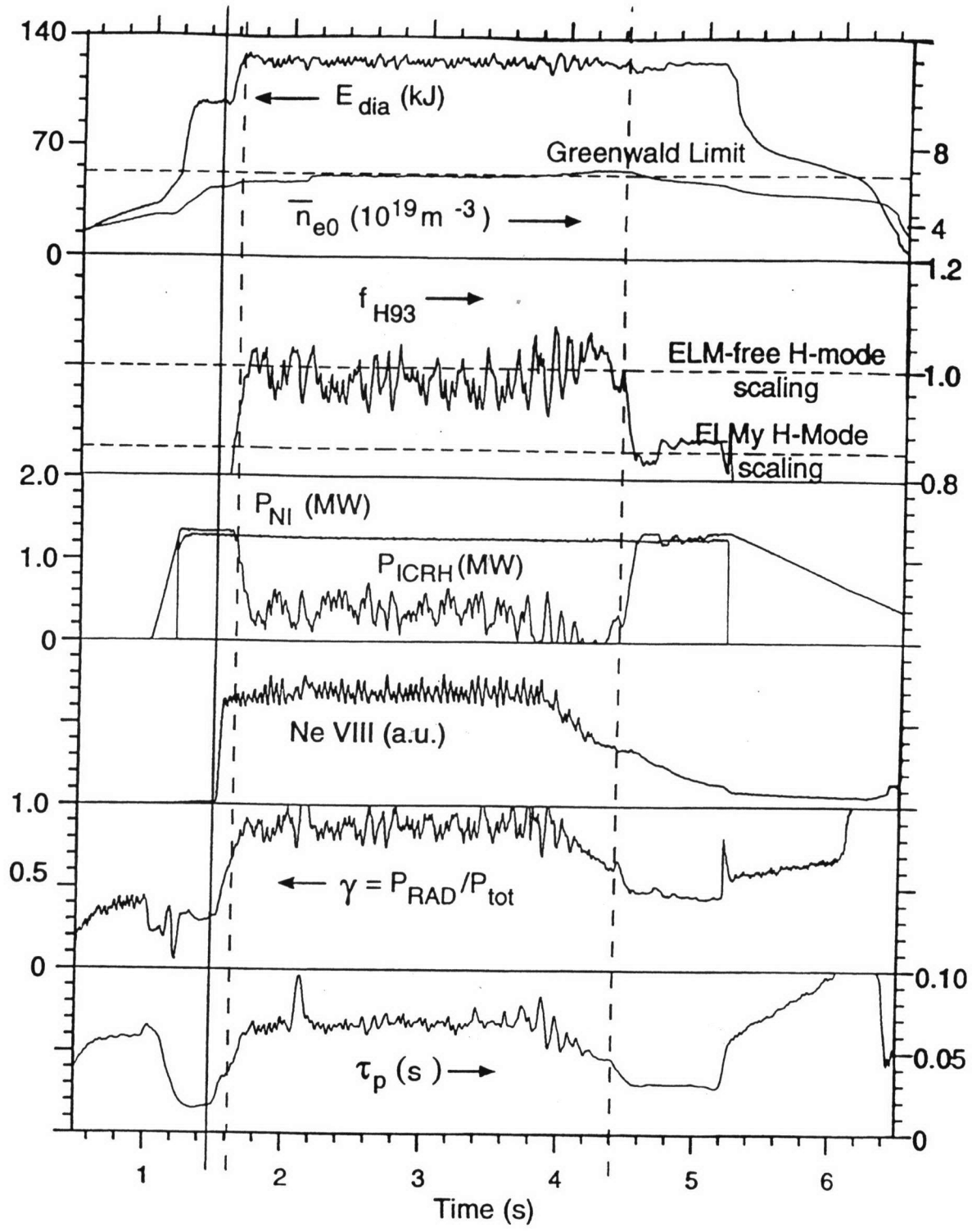

Figure 14: RI mode in Textor with neon seeding. $I_p = 0.4$ MA, B = 2.25 T, shot = 68825.

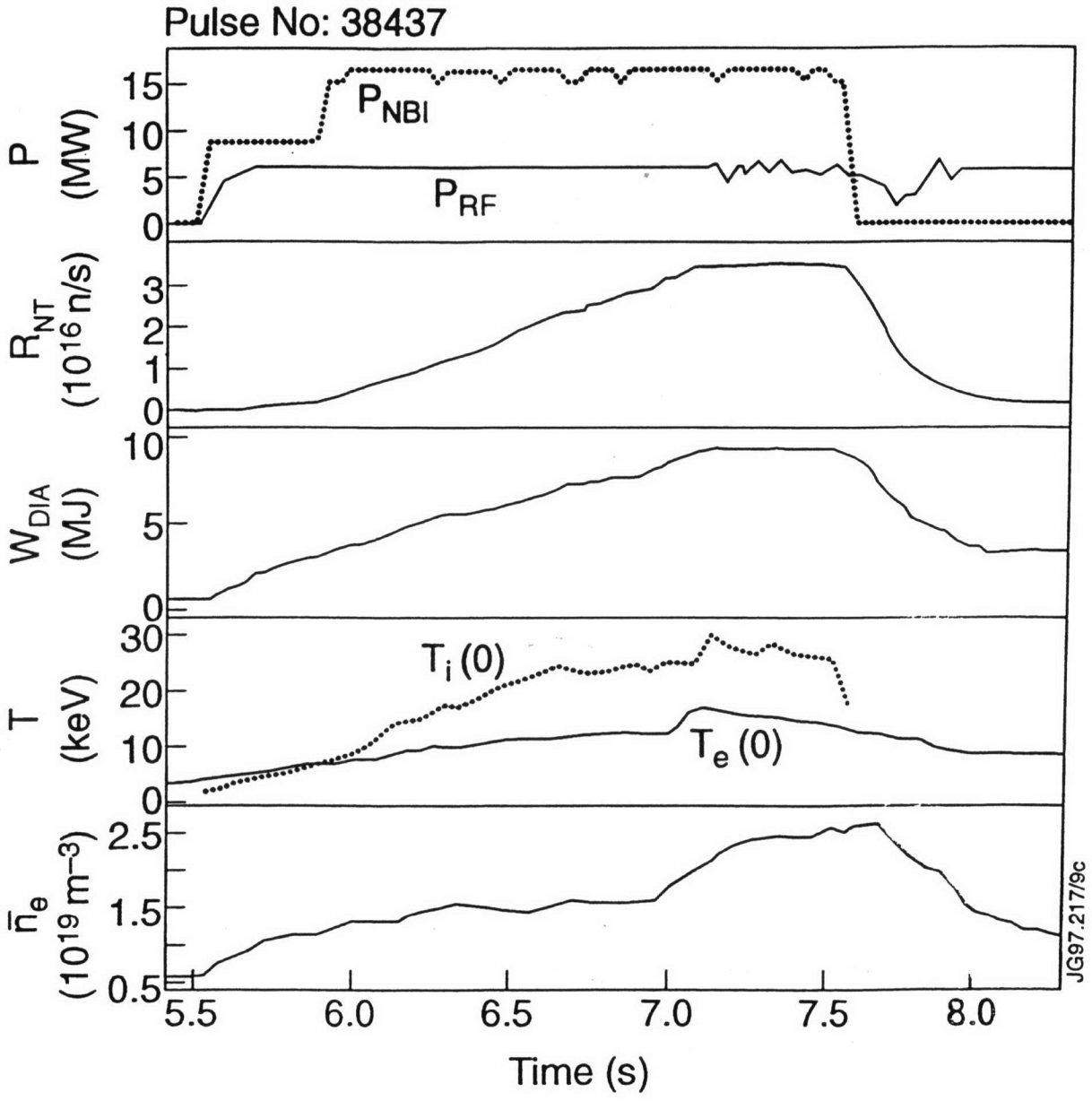

Figure 15: Optimized shear mode in JET with NBI and ICRF.